Build Simul (2023) 16: 557–576
https://doi.org/10.1007/s12273-022-0958-0

Biofuel-driven trigeneration systems for non-residential building applications: A holistic assessment from the energy, environmental and economic perspectives

K.F. Fong (✉), C.K. Lee

Division of Building Science and Technology, College of Engineering, City University of Hong Kong, Tat Chee Avenue, Kowloon, Hong Kong, China

Abstract

In the metropolises, it is unlikely to use merely solar and wind energy to pursue zero carbon building design. However, it would become possible if biofuel-driven trigeneration systems (BDTS) are adopted. It is thus essential to assess the application opportunity of BDTS in a holistic way. In this study, BDTS offered definite primary energy saving of up to 15% and carbon emissions reduction of at least 86% in different types of non-residential buildings as compared to the conventional systems. With 24/7 operation for the hotel and hospital buildings, the corresponding BDTS could even achieve zero carbon emissions. All the BDTS primed with compression-ignition internal combustion engine were not economically viable even in running cost due to the high local biodiesel price level. The BDTS primed with spark-ignition engine and fueled by biogas, however, would have economic merit when carbon price was considered for the conventional systems that fully utilize fossil fuels. Adoption of carbon tax and social cost could have the payback ceilings of 8 years and 2 years respectively for most of building types. Consequently, the results could reflect the application potential of BDTS for non-residential buildings, leading the pathway to carbon neutrality for sustainable sub-tropical cities.

Keywords

trigeneration;
biofuel;
dynamic simulation;
carbon tax;
social cost;
economic analysis

Article History

Received: 05 February 2022
Revised: 18 October 2022
Accepted: 31 October 2022

1 Introduction

With the worldwide awareness of global warming and the quest for a sustainable living, the urge for reduction in carbon emissions has gained primary attention. Indeed, the Hong Kong government has recently announced the targets to cut the energy intensity by 40% by 2025 (EB 2015), and the carbon dioxide emission by 50% by 2035 (EB 2021) both based on the respective levels in 2005. It is further targeted that Hong Kong should reach carbon neutral before 2050. In a densely-populated city like Hong Kong, most of the buildings are multi-storey. Carbon emissions cut through renewable energy sources is not apparent since the available space for installation of such facilities like solar panels or wind turbines are limited. In fact, the local power plants are the major sources of carbon emissions. Moreover, the energy loss in the transmission and distribution systems of a large electric grid is not negligible.

The reduction in the fossil fuel demand through the enhancement of energy efficiency in the power generation and distribution systems is always an important direction of sustainable development. However, this usually requires low-term planning and execution. In effect, distributed power generation at the building level can be a feasible solution. In the hot and humid cities, the adoption of trigeneration systems, which utilize the waste heat from the prime movers to provide, cooling and heating, would be more energy-efficient than the conventional power plants. According to Al-Sulaiman et al. (2010), the overall fuel energy utilization of trigeneration systems could exceed 70%. To further enhance the environmental merit of trigeneration systems, biofuels can be involved to drive the prime movers. A zero carbon approach can then be established as biofuels are considered to be carbon-neutral. Hence, the use of biofuel-driven trigeneration systems (BDTS) can be the most possible way. Parise et al. (2011) conducted energy and

E-mail: bssquare@cityu.edu.hk

List of symbols

A	area (m^2)
a_0, a_1, a_2, a_3	empirical coefficients in Eq. (36)
CDE	carbon dioxide emissions (ton)
COP	coefficient of performance of chiller
c_p	specific heat capacity at constant pressure (kJ/(kg·K))
FI_{pm}	fuel injection rate of prime mover (kg/s)
FIR	fuel injection ratio
H	enthalpy (kJ)
h	specific enthalpy (kJ/kg)
$\dot{m}$	mass flow rate (kg/s)
N_{pm}	number of prime movers in operation
P	pressure (kPa)
P_s	saturated vapor pressure of LiBr solution (kPa)
PEC	primary energy consumption (MWh)
PLR	part-load ratio
$PMEE$	prime mover electrical efficiency (%)
Q	thermal energy (kJ)
$\dot{Q}$	thermal power (kW)
rps	engine speed (rev/s)
S	valve control signal
$SCCO_2$	social cost of carbon dioxide (USD/ton of CO_2)
SP	simple payback (Year)
T	temperature (K or °C)
$\overline{T}$	mean temperature (K or °C)
$tFIR_{els}$	total fuel injection ratio based on equal load sharing
$tFIR_{opt}$	optimal total fuel injection ratio
$t\dot{W}_{demand}$	total electricity demand of building (kW)
UA	overall heat transfer value (kJ/K)
V	volume (m^3)
W_{net}	net work output per engine cycle (kJ)
$\dot{W}_{pm}$	capacity of prime movers (kW)
ΔT_m	log-mean-temperature-difference (K)
ϕ	shaft rotation angle during the combustion process (degree)
γ	ratio of specific heat capacity of ideal gas
ξ	LiBr solution concentration (kg/kg)
σ	Stefan-Boltzmann constant (5.67×10^{-11} kW/(m^2·K^4))

Subscripts

1–4	different state points for the diesel and gas engine cycles
AbCV	absorption chiller regenerative hot water control valve
AWCV	auxiliary water cooler control valve
ab	absorber
abw	absorber water
ai	absorber inlet
amb	ambient
ao	absorber outlet
cas	engine casing
chw	chilled water
chwr	chilled water return
cond	condenser
cw	cooling water
cyl	engine cylinder
dis	refrigerant discharge from the generator
evap	evaporator
f	fuel
gen	generator
gi	generator inlet
go	generator outlet
hw	hot water
i	inlet
jac	engine jacket
jw	engine jacket water
max	maximum
nom	nominal
o	outlet
r	refrigerant
rhwr	regenerative hot water return
SACV	supply air cooling valve
SAHV	supply air heating valve
s	LiBr solution
sc	setpoint for cooling
sh	setpoint for heating
sshxr	solution-to-solution heat exchanger
suc	refrigerant suction into the absorber
w	water
zone	building zone

Abbreviations

1	gas state inside the cylinder at the beginning of the compression stroke
2	gas state inside the cylinder at the end of the compression stroke
3	gas state inside the cylinder at the end of the combustion process
4	gas state inside the cylinder at the end of the expansion stroke
AbCV	absorption chiller control valve
AbCWP	absorption chiller cooling water pump
AbChWP	absorption chiller chilled water pump
AJWCV	auxiliary jacket water cooler valve
BDTS	biofuel-driven trigeneration systems
CCW	conventional chilled water
CI	compression-ignition engine
DO	diesel oil

EEHX	engine exhaust heat exchanger	SAF	supply air fan
EEHXV	engine exhaust heat exchanger valve	SAH	supply air heating coil
EJHX	engine jacket heat exchanger	SC	sports center
EJWP	engine jacket water pump	SAHV	supply air heating coil valve
HP	hospital building	SHHX	space heating heat exchanger
HT	hotel building	SHHXV	space heating heat exchanger valve
NA	not applicable	SHWP	space heating water pump
OF	office building	SI	spark-ignition engine
RHWP	regenerative hot water pump	SSP	shared socioeconomic pathways
RT	retail building	TG	town gas
S1	economic analysis without carbon price	VCCWP	vapor-compression chiller condenser water pump
S2	economic analysis including carbon tax		
S3	economic analysis including carbon social cost	VCChWP	vapor-compression chiller chilled water pump
SAC	supply air cooling coil	WHHX	water heating heat exchanger
SACV	supply air cooling coil valve	WHHXV	water heating heat exchanger valve

environmental assessment of biodiesel trigeneration system with prime mover of compression-ignition internal combustion engine, as compared to the conventional provisions. It was found that significant reduction on primary energy consumption and carbon emissions could be attained. Use of biodiesel has become popular, like the adoption of non-edible plant oils to energize trigeneration systems for building applications (Wang et al. 2010; Hossain et al. 2011; Wu et al. 2013; Wu et al. 2015). In Hong Kong, there is a demonstration project of biodiesel trigeneration in Zero Carbon Building (ZCB 2022), in which various passive and active sustainable means are designed to achieve zero carbon target for building in hot-humid climate (Li 2012). Biogas can also be considered for the popular prime movers, like spark-ignition internal combustion engine and gas turbine. Biogas can be generated from anaerobic sludge digestion in wastewater treatment, and used in cogeneration or trigeneration for power supply (Nowak et al. 2015; Nourin et al. 2021).

At present, the supply of biofuel in Hong Kong generally falls into two main categories, biodiesel and biogas. There are three companies which have production at their plants in Hong Kong. They collect the waste/used cooking oil, animal fat and grease trap oil as feedstocks from the restaurants and convert it to biodiesel. About biogas, there are several sites which provide landfill gas to the local gas company for further treatment before delivery to the users. Strategically, landfill gas is provided directly from one landfill site to a nearby hospital building for driving a cogeneration system (SCMP 2015). A large-scale organic waste treatment plant was commissioned in 2018 (OPARK1 2020), and biogas can be produced and utilized for power generation for use by 3000 households. Unlike the landfill gas, the supply of biogas from the organic waste treatment facilities can last through the operating life of the plant. Actually, the biogas generated from the sewage treatment is effective to be applied for trigeneration systems (Chen et al. 2016a; Chen et al. 2016b; Dehghani and Yoo 2020).

Wang et al. (2013a) highlighted the significance of trigeneration as distributed power generation for residential buildings. Wang et al. (2013b) also evaluated BDTS for residential building application to meet changing load demands throughout a year. Ren et al. (2010) considered demand side characteristics and investigated an optimal design of biogas trigeneration system for a residential area. It was found that there were noticeable influences of the key parameters on the system, including electricity and city gas tariffs, biogas price, electricity buy-back price and carbon tax rate. Studies about trigeneration were also made for non-residential buildings, but only a certain building type was involved in energy and environmental assessment (Gazda and Stanek 2016; Meyers et al. 2016; Taseli and Kilkis 2016). Economic analysis regarding the consideration of carbon price was seldom conducted. In addition, demand of auxiliary grid power was commonly ignored. Actually most of the non-residential buildings are not in 24/7 operation. Hence, at night, the electricity demand, which mainly comes from lighting, will be very low as compared to that at the day time when air-conditioning system is switched on. If this small electricity demand is also provided by the BDTS, it will need to be operated in a very low part-load ratio. Moreover, the BTDS will then only be a power generator instead of a trigeneration system and all the waste heat will just be dissipated to the ambient without utilization. This does not seem to be a good choice particularly when the economic merit of the trigeneration is considered. Accordingly, auxiliary grid power will be utilized to serve the low electricity demand at night time. In this regard, it is necessary to fully investigate the application potential of BDTS for various types of non-residential

buildings. Analyses should be made not only on the energy and environmental aspects, but also on the economic situation of the BDTS with the concern of carbon price. In this connection, five types of multi-storey buildings, namely office (OF), hotel (HT), retail (RT), hospital (HP) and sports center (SC) were considered in this study. They represent different cooling-to-heating-to-power ratios among the non-residential premises in the subtropical Hong Kong. Internal combustion engines were applied, since they are the most feasible types of prime movers within the capacity range of building application. Moreover, they generally offered higher electrical efficiency [critical in consideration of the benefits of the trigeneration systems according to a previous study (Fong and Lee 2017)] that other types of common prime movers within the capacity range considered. For the thermally-driven cooling equipment, LiBr absorption chiller was selected since absorption chiller would offer better energy efficiency (also important in consideration of the benefit of the trigeneration systems) over a wide range of weather conditions according to Fong et al. (2010), and that LiBr was the most common solution for absorption chiller. To conduct this study, year-round dynamic system simulation would be adopted, so that the part-load performances of different equipment in the BDTS can be reflected. Through this study, it is expected to work out the energy, environmental and economic features of BDTS in the sub-tropical climate.

2 Model formulation

Most of the component models required are available in TRNSYS (TRNSYS 2011). They include vapor compression chiller, cooling tower, air-handling unit, multi-zone building. Only the models for the internal combustion engines and the absorption chillers need to be developed.

2.1 Internal combustion engines

There are generally two types of internal combustion engines, namely the compression-ignition engine (CI) and the spark-ignition engine (SI). The modeling approaches for the CI and SI detailed in Fong and Lee (2015) based on the four-stroke cycle analyzes were used in this study. Here, 1→2 is the compression stroke, 2→3 the combustion stroke, 3→4 the expansion stroke and 4→1 the discharge stroke. Both the compression and expansion processes were assumed to be isentropic. For the SI, an isobaric combustion was undergone with the fuel injected into the cylinder at the end of the compression stroke. Meanwhile, for the SI, the fuel was mixed with the intake air before the start of the compression stroke, and the combustion process was isochoric. To simplify the analysis, it was assumed that the transfer of heat to the engine jacket and the environment only existed in the combustion process based on an average cylinder temperature calculated throughout the entire cycle. Moreover, the combustion process was assumed to be complete. The CI ran on biodiesel which was taken as decane. The SI was fueled by biogas which was assumed to be pure methane. The model formulation was briefed as follows:

For the compression and expansion processes,

$$\frac{P_2}{P_1}=\left(\frac{V_1}{V_2}\right)^{\gamma}=\left(\frac{T_2}{T_1}\right)^{\frac{\gamma}{\gamma-1}} \tag{1}$$

$$\frac{P_4}{P_3}=\left(\frac{V_3}{V_4}\right)^{\gamma}=\left(\frac{T_4}{T_3}\right)^{\frac{\gamma}{\gamma-1}} \tag{2}$$

For the constant-pressure combustion in the CI engine,

$$H_3=H_2+H_f-Q_{\text{jac}}-Q_{\text{amb}}-P_2\left(V_3-V_2\right) \tag{3}$$

For the constant-volume combustion in the SI engine,

$$H_3=H_2+H_f-Q_{\text{jac}}-Q_{\text{amb}} \tag{4}$$

To evaluate the heat loss to the engine jacket (Q_{jac}) and the environment (Q_{amb}), an average cylinder temperature ($\overline{T}_{\text{cyl}}$) was determined and individual heat transfer values were employed to calculate the convective heat transfers between the cylinder and the engine jacket (UA_{jac}) as well as that between the engine jacket and the ambient (UA_{amb}). The radiative heat transfer between the engine jacket and the ambient was also taken into account. These heat losses were assumed to occur only within the combustion process in order to determine the peak cylinder temperature at the end of the combustion stroke. Consequently,

$$Q_{\text{jac}}=\frac{2UA_{\text{jac}}\left(\overline{T}_{\text{cyl}}-\overline{T}_{\text{jw}}\right)}{rps}=\frac{2\dot{m}_{\text{jw}}c_{\text{p,jw}}\left(T_{\text{jw,o}}-T_{\text{jw,i}}\right)}{rps} \tag{5}$$

$$Q_{\text{amb}}=\frac{2}{rps}\left[UA_{\text{amb}}\left(\overline{T}_{\text{cas}}-T_{\text{amb}}\right)+\sigma A_{\text{cas}}\left(\overline{T}_{\text{cas}}^4-T_{\text{amb}}^4\right)\right] \tag{6}$$

$$\overline{T}_{\text{jw}}=\frac{T_{\text{jw,i}}+T_{\text{jw,o}}}{2} \tag{7}$$

$$\overline{T}_{\text{cas}}=\frac{\overline{T}_{\text{cyl}}+\overline{T}_{\text{jw}}}{2} \tag{8}$$

For the CI engine,

$$\overline{T}_{\text{cyl}}=\frac{180\left(T_1+T_4\right)+180\left(T_1+T_2\right)+\phi\left(T_2+T_3\right)+\left(180-\phi\right)\left(T_3+T_4\right)+360T_4}{1440} \tag{9}$$

$$\phi=\cos^{-1}\left(1-\frac{2\left(V_3-V_2\right)}{V_1-V_2}\right) \tag{10}$$

For the SI engine,

$$\overline{T}_{cyl} = \frac{180(T_1 + T_4) + 180(T_1 + T_2) + 180(T_3 + T_4) + 360T_4}{1440} \tag{11}$$

and the cylinder pressure at the end of the combustion process could be determined from

$$\frac{P_3}{P_2} = \frac{T_3}{T_2} \tag{12}$$

The net work output per cycle for both types of engines was given by

$$W_{net} = H_3 - H_4 - H_2 + H_1 + P_2(V_3 - V_2) \tag{13}$$

It should be noted that $V_2 = V_3$ for the SI engine. To calculate the engine performance, the clearance volume (V_2), swept volume ($V_1 - V_2$), engine speed (*rps*), engine casing area (A_{cas}), the two overall heat transfer values and the jacket water mass flow ($\dot{m}_{jw}$) were specified. At given fuel injection rate, ambient temperature (T_{amb}) and jacket water inlet temperature ($T_{jw,i}$), an iterative approach was used to determine the overall engine performance.

Comparison of the engine models was made with the sample data in TRNSYS for the trigeneration genset based on the rated capacity, efficiency, heat loss to jacket and heat loss to surrounding under the same volumetric compression ratio and fuel injection rate. The results were close to each other, thus the engine models were validated. In this study, it was understood that the engine models were simplified. Hence, it might not fully reflect the actual behavior of the prime movers during the non-rated operations. Nevertheless, it at least provided a useful comparison of the relative performances of the BDTS used in different building types.

2.2 Single-effect LiBr absorption chiller

Fong et al. (2012) previously outlined a model for a single-effect LiBr absorption chiller based on Florides et al. (2003) as shown in Figure 1, which could be briefed as follows:

By applying the energy and mass balance in the generator,

$$\dot{Q}_{gen} = \dot{m}_{hw} c_{p,w} (T_{hw,i} - T_{hw,o}) = UA_{gen} \Delta T_{m,gen} \tag{14}$$

$$\text{where} \quad \Delta T_{m,gen} = \frac{(T_{hw,o} - T_{s,gi}) - (T_{hw,i} - T_{s,go})}{\ln\left(\frac{T_{hw,o} - T_{s,gi}}{T_{hw,i} - T_{s,go}}\right)} \tag{15}$$

$$\dot{Q}_{gen} + \dot{m}_{s,ao} h_{s,gi} = \dot{m}_{s,go} h_{s,go} + \dot{m}_r h_{r,dis} \tag{16}$$

$$\dot{m}_{s,ao} \xi_{s,ao} = \dot{m}_{s,go} \xi_{s,go} \tag{17}$$

$$\dot{m}_r = \dot{m}_{s,ao} - \dot{m}_{s,go} \tag{18}$$

$$P_{r,cond} = P_s(T_{s,go}, \xi_{s,go}) \tag{19}$$

The heat and mass transfer in the absorber was determined from

$$\dot{Q}_{ab} = \dot{m}_{abw} c_{p,w} (T_{abw,o} - T_{cw,i}) = UA_{ab} \Delta T_{m,ab} \tag{20}$$

$$\text{where} \quad \Delta T_{m,ab} = \frac{(T_{s,ao} - T_{cw,i}) - (T_{s,ai} - T_{abw,o})}{\ln\left(\frac{T_{s,ao} - T_{cw,i}}{T_{s,ai} - T_{abw,o}}\right)} \tag{21}$$

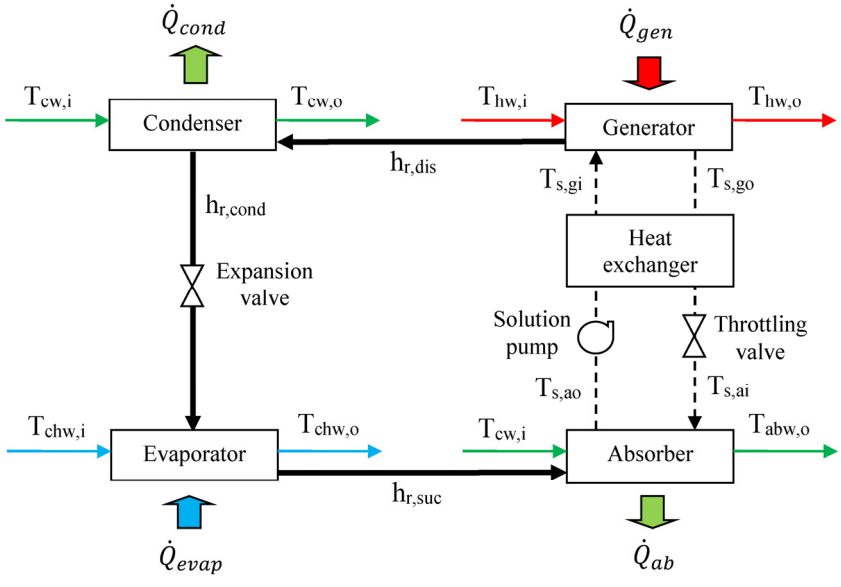

Fig. 1 Schematic diagram of the absorption chiller

$$\dot{Q}_{ab} + \dot{m}_{s,ao} h_{s,ao} = \dot{m}_{s,go} h_{s,ai} + \dot{m}_{r} h_{r,suc} \quad (22)$$

$$P_{r,evap} = P_{s}\left(T_{s,ao}, \xi_{s,ao}\right) \quad (23)$$

With no change in states in the flow streams, the performance of the solution-to-solution heat exchanger can simply be calculated from

$$\dot{m}_{s,ao} c_{p,s,ao}\left(T_{s,gi} - T_{s,ao}\right) = \dot{m}_{s,go} c_{p,s,go}\left(T_{s,go} - T_{s,ai}\right) = UA_{sshxr} \Delta T_{m,sshxr} \quad (24)$$

$$\text{where} \quad \Delta T_{m,sshxr} = \frac{\left(T_{s,ai} - T_{s,ao}\right) - \left(T_{s,go} - T_{s,gi}\right)}{\ln\left(\frac{T_{s,ai} - T_{s,ao}}{T_{s,go} - T_{s,gi}}\right)} \quad (25)$$

The modeling methods adopted by Lee and Lam (2014) were used for the condenser and the evaporator. Each coil was divided into maximum three portions corresponding to the different states of the refrigerant (sub-cooled, saturated or superheated) and the complete coil performance was calculated using a simplified explicit approach. In general,

$$\dot{Q}_{cond} = \dot{m}_{cw} c_{p,w}\left(T_{cw,o} - T_{cw,i}\right) \quad (26)$$

$$\dot{Q}_{evap} = \dot{m}_{chw} c_{p,w}\left(T_{chw,i} - T_{chw,o}\right) \quad (27)$$

$$COP = \frac{\dot{Q}_{evap}}{\dot{Q}_{gen}} \quad (28)$$

The complete absorption chiller performance was determined by solving Eqs. (14)–(28) iteratively. The overall heat transfer values for the generator, absorber, condenser, evaporator, and solution-to-solution heat exchanger together with the mass flow rates of the cooling water, chilled water and solution at absorber discharge were specified. The chiller performance at different hot water, cooling water and chiller water entering temperatures as well as the hot water mass flow rate was then evaluated. To enhance the stability of the calculation, an equivalent-capacitance approach as proposed by Lee and Lam (2014) was used instead of the log-mean-temperature-difference approach to calculate the heat transfer in the generator and the absorber. To validate the model, a sample comparison was made with that from Heriod et al. (2016) with close agreement found.

3 System description

3.1 System configuration

Figure 2 shows the schematic diagram of the BDTS considered in this study including the design temperature levels at various positions. Waste heat was collected through the engine jacket heat exchanger (EJHX) and the engine exhaust heat exchanger (EEHX). The regenerative water was used to drive an absorption chiller through an absorption chiller control valve (AbCV). A space heating heat exchanger (SHHX) was added between regenerative water and space heating water streams in order to maintain different temperature levels for the two water streams. Meanwhile, a water heating heat exchanger (WHHX) was employed to separate the regenerative water and the potable water in fulfilment of the statutory requirement. In case there was no cooling and heating demand when the generator was

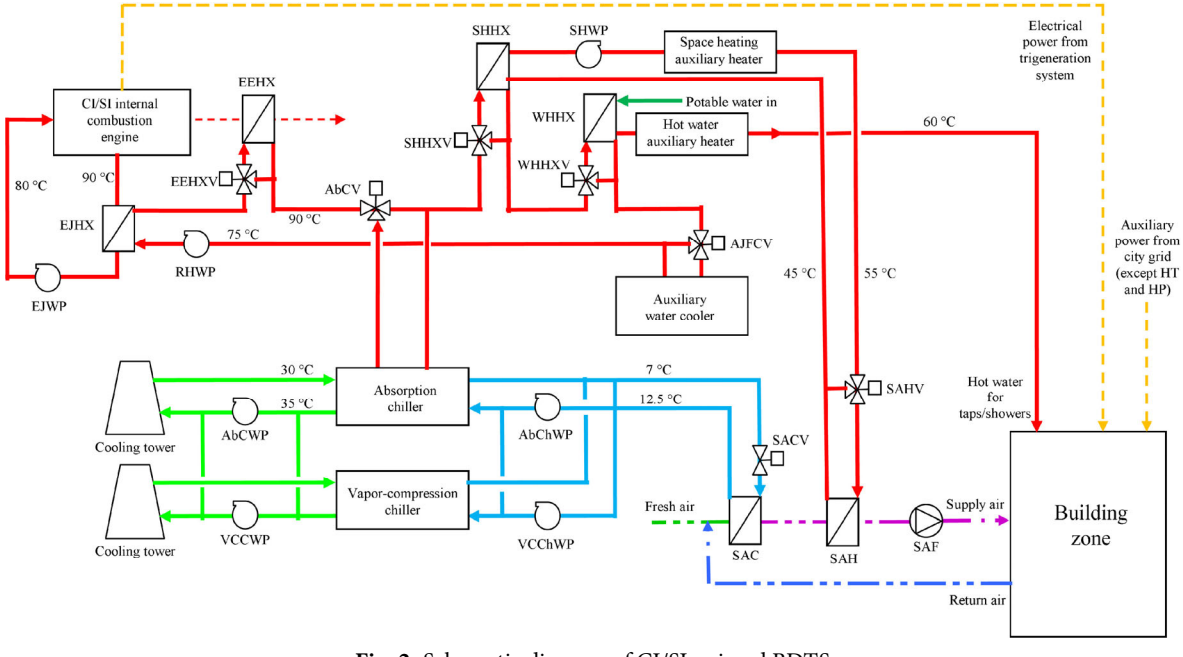

Fig. 2 Schematic diagram of CI/SI-primed BDTS

running, an air-cooled type auxiliary water cooler was needed to maintain the jacket water temperature to the design level. In this circumstance, the regenerative hot water would bypass the EEHX by shutting the engine exhaust heat exchanger valve (EEHXV).

In a sub-tropical climate, the ratio of peak cooling load to peak electrical load of the building was large, and the capacity of the absorption chiller might not be sufficient to satisfy all the air-conditioning demand. Hence, auxiliary vapor-compression chillers were provided to supplement the deficit chiller capacity. The corresponding condenser water pumps (AbCWP, VCCWP), cooling towers and chilled water pumps (AbChWP, VCChWP) were provided for each chiller. The chilled water pumps supplied chilled water to the supply air cooling coil (SAC) through the supply air cooling valve (SACV). Meanwhile, space heating water was circulated by the space heating water pump (SHWP) to the supply air heating coil (SAH) through the supply air heating valve (SAHV). To ensure that the required water temperatures were reached for space and water heating, individual auxiliary heaters which also ran on biofuel were employed.

The electricity demands in the buildings mainly came from lighting, electrical office equipment, lifts and other building services facilities like auxiliary vapor-compression chillers, cooling towers, water pumps and supply air fans of air handling units. For the building types OF, RT and SC, there was no activity inside the buildings during the night time. The corresponding electricity demand became very low. To avoid the BDTS to be operated at a very low part-load ratio, auxiliary electricity supply from the grid was used to fulfil the demand during the said period rather than switching on the BDTS. For benchmarking, the configurations of the conventional chilled water (CCW) systems were similar to those of the BDTS except that only water-cooled vapor-compression chillers are used. Besides, electric heaters were employed for space heating rather than primary ones when applied to the OF due to the limited usage.

3.2 System control strategies

For effective operation of the BDTS, the various parts of the system should be suitably controlled for optimal performance. These included the switching and modulation of the prime movers, absorption chillers, auxiliary vapor-compression chillers and the auxiliary water cooler as well as the functioning of the space cooling/heating and water heating systems as detailed below.

3.2.1 *Prime mover*

In this study, the follow-electricity-demand approach was adopted. The reason was that as mentioned in Section 3.1, the waste heat from the prime movers were not sufficient to provide the required cooling demand. Hence, if a follow-heat-demand approach was adopted, the BDTS would most likely be operated at full load during the day time. This would cause a huge surplus of electricity supply during the said period unless it could be fed back to the grid at a reasonable price. As there was no such scheme in Hong Kong for biofuel generator, only the follow-electricity-demand was considered. In other words, the electrical output of the prime movers should meet exactly the building demand. By estimating the total electricity demand of the building ($t\dot{W}_{\text{demand}}$), the number of prime movers employed (N_{pm}) was given by

$$N_{\text{pm}} = \text{Min}\left[\text{Int}\left(\frac{t\dot{W}_{\text{demand}}}{\dot{W}_{\text{pm,nom}}}\right)+1, N_{\text{pm,max}}\right] \tag{29}$$

where Int( ) was the integer part of the expression, $\dot{W}_{\text{pm,nom}}$ was the nominal capacity of each prime mover and $N_{\text{pm,max}}$ was the maximum number of prime movers.

It might be queried how the prime movers could response to rapid power fluctuation. It was a common consequence that power generator sets used in remote application like a construction site should encounter a rapid power fluctuation in actual practice. Hence, they should be equipped with suitable facilities to handle this situation. In the present system specifications, there was always electricity demand throughout the year. Besides, when there was heating load, whether space heating or water heating, there should always be some equipment that need to be switched on in order to provide the heating.

Upon determination of the number of prime movers to be energized, the next step was the calculation of the fuel input required. In case more than one prime mover was used, the load sharing among the prime movers needed to be set first. An optimization study was needed to determine the optimal strategy for that before the actual system analysis was made. Figure 3 shows the control algorithm of the prime movers.

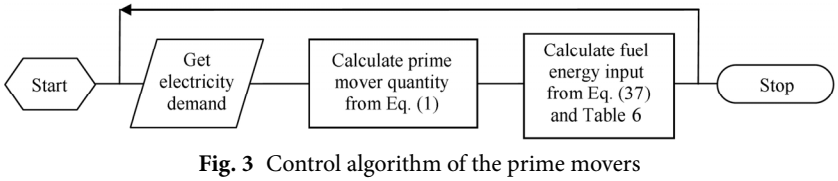

Fig. 3 Control algorithm of the prime movers

3.2.2 *Chiller plant*

The operation of the chiller plant was governed by a thermostat triggered by the return chilled water temperature (T_{chwr}) between 9.5 and 12.5 °C as shown in Figure 4. To minimize the utilization of the auxiliary chillers, the absorption chillers were operated with priority. Hence, the algorithms for the sequencing of the absorption and vapor-compression chillers were different as shown in Figure 5. To facilitate the system design, the number of absorption chillers used would be the same as the number of prime movers employed. It was to ensure that the hot water temperature entering the absorption chillers was sufficiently high and that the hot water flow rate was enough. In this regard, the maximum number of available absorption chiller was also taken to be the same as the number of operating prime movers when determining the stepping up of vapor-compression chillers.

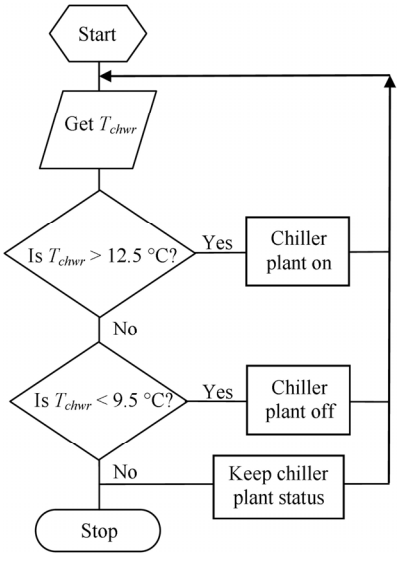

Fig. 4 Control algorithm of chiller plant

To simplify the analysis, all operating absorption chillers were assumed to perform in the same manner as well as all the operating vapor-compression chillers. With the chillers switched on, the corresponding chilled water and condensing water pumps were turned on. Regarding the cooling towers, they were additionally governed by a thermostat triggered by the return condenser water temperature between 15 and 20 °C in the similar way as the return chilled water thermostat as previously indicated in Figure 4. To optimize the operation of the chiller plant, part-load control was employed for both types of chillers. For the absorption chiller, the entering regenerative hot water flow rate was regulated through the absorption chiller control valve in accordance with the following equation:

$$S_{\mathrm{AbCV}} = \mathrm{Max}\left\{\mathrm{Min}\left[1-\left(12.5-T_{\mathrm{chwr}}\right)/3,1\right],0.5\right\} \tag{30}$$

Regarding the vapor-compression chiller, it was assumed to be modulated automatically such that a constant chilled water supply temperature of 7 °C could be maintained. The chillers could run in part-load but with a preset minimum value of 50%. Hence, the number of operating chillers depends on the system cooling demand with could vary with time. This was the situation in real practice. Of course, suitable control could be made so that the operating time of each chiller was similar and that the switching on and off ofndividual chiller would not occur within a short period of time.

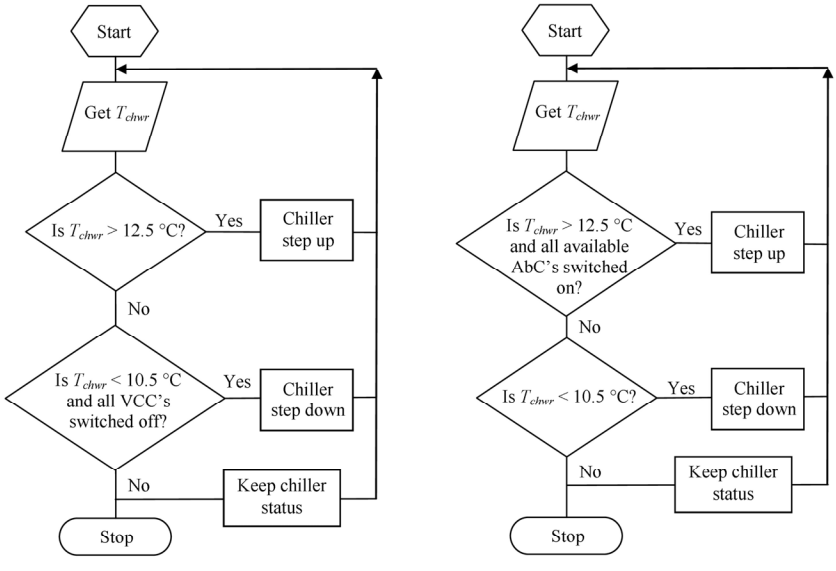

(a) Absorption chiller (b) Vapor-compression chiller

Fig. 5 Control algorithm for chiller sequencing

3.2.3 *Waste heat recovery system*

Figure 6 depicts the control algorithm of the waste heat recovery system. It was assumed that each prime mover was equipped with individual RHWP which was energized when the respective prime mover was put into operation. The regenerative hot water return temperature (T_{rhwr}) was used to control the operation of the auxiliary water cooler and hence the EEHXV through a reverse acting thermostat between 75 and 80 °C. With the auxiliary water cooler on, the AWCV was controlled proportionally as shown below:

$$S_{AWCV} = \text{Max}\left\{\text{Min}\left[\left(T_{rhwr} - 75\right)/5, 1\right], 0.1\right\} \quad (31)$$

The space heating system was controlled by the ambient temperature (T_{amb}) which functioned when the ambient temperature was less than 22 °C. Meanwhile, the hot water heating system was always put into operation.

3.2.4 *Air-conditioning system*

The supply air cooling and heating valves were controlled by respective proportional controllers based on the zone temperature (T_{zone}) in the following manners.
For SACV,

$$S_{SACV} = \text{Max}\left[\text{Min}\left(T_{zone} - T_{sc}, 1\right), 0.3\right] \text{ when } T_{zone} > T_{sc} \quad (32)$$

For SAHV,

$$S_{SAHV} = \text{Max}\left[\text{Min}\left(T_{sh} - T_{zone}, 1\right), 0.3\right] \text{ when } T_{zone} < T_{sh} \quad (33)$$

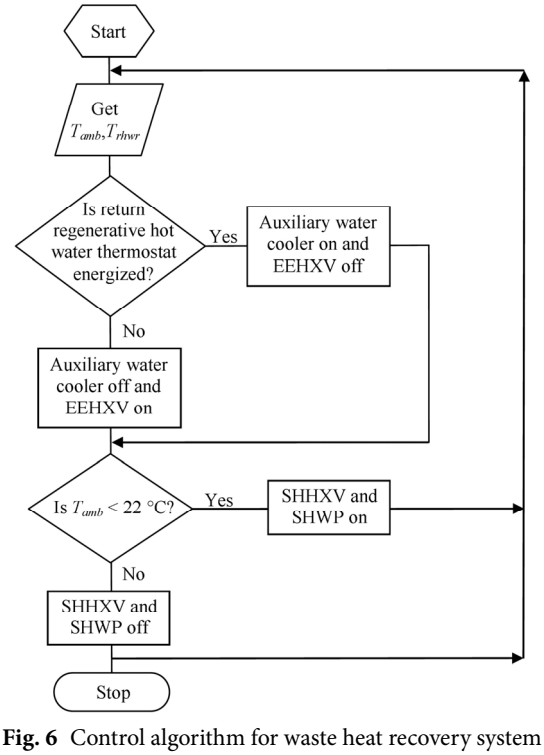

Fig. 6 Control algorithm for waste heat recovery system

where T_{sc} was the zone cooling set point and T_{sh} was the zone heating set point.

3.3 System specification

Figure 7 show the respective floor plans for the reference office, hotel, retail and hospital buildings, as well as the reference sports center adopted, the first three being based on EMSD (2007). The reference office building was 30-storey high with a size of 40.8 m × 40.8 m for each floor. The exterior zone was defined as the region within 4 m from the building external wall. The reference hotel building was 20-storey high. Each guestroom had a size of 4 m × 8 m and the corridor was 2 m wide. The reference retail building was 4-storey high (three floors for shops and one floor for restaurants) with a size of 60 m × 36 m for each floor. The corridor was 3 m wide. Both the interior and exterior zones are defined as the regions within 4.5 m from the both sides of corridor. For the restaurant floor, the corridor was included in the interior zone. The reference hospital building was 10-storey high, which had a size of 75.5 m × 15 m and consisted of two wings and connected by a central common lift lobby. The reference sports center comprised an indoor games hall of size 42 m (L) × 35 m (W) × 9 m (H) and a back of house of 2-storey high with a size of 6 m (L) × 35 m (W). The upper storey contained the plant rooms while the lower one accommodated the changing rooms and offices.

The year-round cooling, heating and power patterns differ substantially among the five types of buildings. For the office building, there was no occupant at mid-night and during Sunday. The daily peak air-conditioning demand basically coincided with the peak power demand. The hot water demand was negligible and space heating demand was small. For the hotel building, there were occupants throughout the whole day including the night time. The peak air-conditioning demand at mid-day was high but the power demand was small due to the low occupancy during the said period. Space heating demand was higher due to the lower internal heat sources in the guestrooms and the higher fresh airflow rate. The demand for hot water spread throughout the whole day with the peaks occurred in the morning after wake up and at night before sleeping. For the retail building, there was no occupant at mid-night but the occupancy was high during Sunday. Space heating demand was similar to that for the office building but the hot water demand was comparable to that for the hotel building and spread over the entire period of the day. The demand patterns for cooling, heating and power for the hospital building were the same for each day of the year. Air-conditioning was required continuously throughout the whole year. As the fresh air demand for the hospital building was

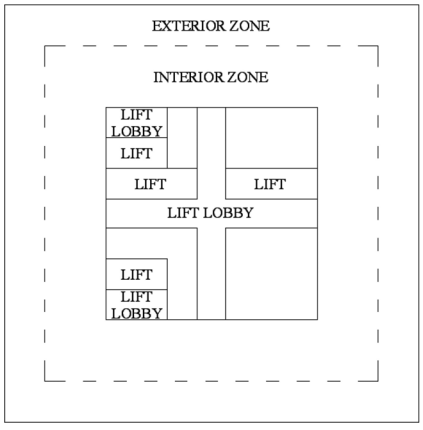

(a) Floor layout of the reference office building

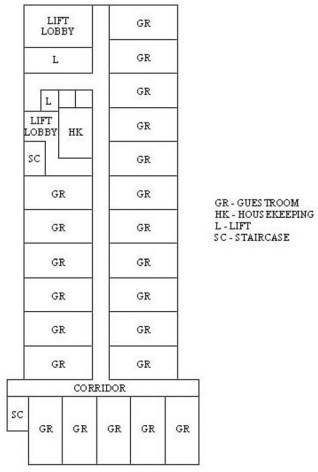

(b) Floor layout plan of the reference hotel building

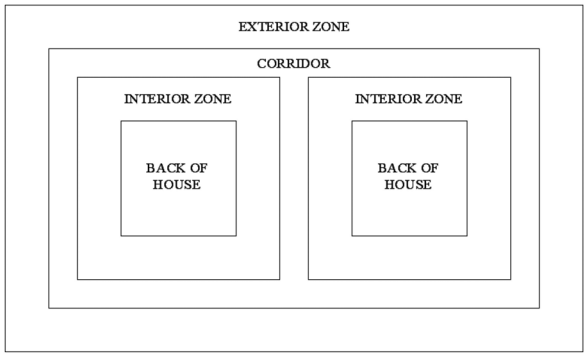

(c) Floor layout plan of the reference retail building

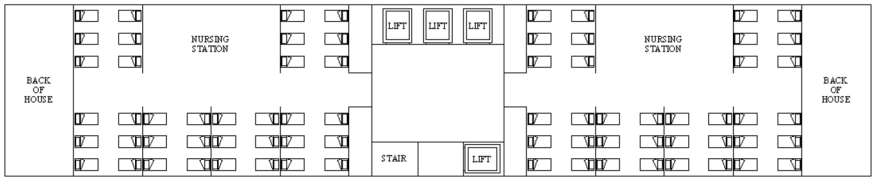

(d) Floor layout plan of the reference hospital building

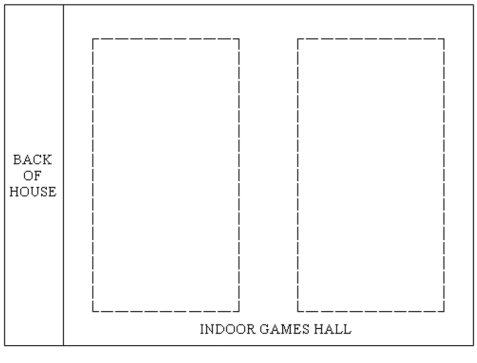

(e) Floor layout plan of the reference sports center

Fig. 7 Floor layout plan of the reference buildings

substantially higher, the respective space heating load was also the highest among the various types of buildings considered. The sports center opened daily from the morning to the evening with no occupancy at mid-night. Compared with the other types of buildings, the equipment load was minimal with no lifts provided.

The air-conditioning demand (including both space cooling and heating) was determined by applying the

respective internal load densities and schedules as detailed in EMSD (2007) and summarized in Table 1 for the various building types. The typical weather data in Hong Kong (Chan et al. 2006) was applied for calculating the heat transfer across the boundary walls and windows. By using the system simulation software TRNSYS, the complete year-round air-conditioning profile was then generated. The design conditions for cooling were 24 °C db and 54% RH, while that for heating was 21 °C db according to EMSD (2012) for the reference office, hotel and retail buildings. For the reference hospital building, the respective design indoor conditions for cooling were 24 °C db and 60% RH, while that for heating was 24 °C db. Regarding the reference sports center, the set conditions for cooling were taken as 22 °C db and 60% RH.

For the reference hotel building adopted with no dining facilities provided, most of the hot water demand came from washing and bathing in the guestrooms. The peak demand was taken as 500 W/person according to EMSD (2007) together with the operating schedules. For the reference retail building, hot water was provided at the restaurant floor for washing and cleaning. The total daily water consumption is 60 L/person distributed throughout the day according to the operating schedules for Chinese restaurants in EMSD (2007). Hot water demand in the reference hospital building came from the shower heads and taps with design water flow rates of 0.11 L/s and 0.15 L/s respectively. The operating periods for each bath from the shower heads and washing from the taps were assumed to be 300 seconds and 33 seconds respectively with the peak utilization rate per hour being two and five. Three taps were provided at the both the hospital corridor and the nursing station, while five taps and three shower heads at the back of house. Only shower heads were considered in the reference sports center with a total amount of 20 sets located at the back of house.

The electrical power demands for lighting and equipment were determined from Table 1. The number of lifts used for the reference office and hospital buildings was four, while it was three for the reference hotel and retail buildings. The power rating of each lift was taken as 40 kVA with a power factor of 0.85 according to EMSD (2012). Regarding the power demand for the air-conditioning equipment, it depended on the system design. The *COP* of the vapor-compression chillers followed the minimum values as stated in EMSD (2012) for screw chillers. Table 2 shows the

Table 1 Summarized air-conditioning loads for the various building types.

Loading type	OF	HT	RT	HP	SC
Maximum occupancy	8 m^2/person	2 persons/room	10 m^2/person at retail floors; 1.4 m^2/person at restaurant floor with 2/3 of floor area for seating	3 persons/bed at cubicle area; 8 m^2/person at nursing station; 10 m^2/person at lift lobby	3 m^2/person at games hall; 4 m^2/person at back of house
Maximum lighting load	20 W/m^2	18 W/m^2	18 W/m^2	17 W/m^2 at cubicle area and nursing station; 13 W/m^2 at back of house; 15 W/m^2 elsewhere	17 W/m^2 at games hall; 13 W/m^2 at back of house
Maximum equipment load	10 W/m^2	900 W/room	30 W/m^2	13 W/m^2 at cubicle area; 30 W/m^2 at nursing station	NA
Fresh airflow	8 L/s/person	30 L/(s·room)	8 L/(s·person)	13 L/(s·person) at cubicle area; 1 L/(s·m^2) at ward corridor; 10 L/(s·person) at nursing station and lift lobby	13 L/(s·person) at games hall; 8 L/(s·person) at back of house

Remark: NA refers to not applicable.

Table 2 Summarized loadings for the various building types

Loading type	OF	HT	RT	HP	SC
Peak power demand excluding air-conditioning system (kW)	1265	620	501	402	24.9
Peak power demand from chillers (kW)	1015	386	507	434	134
Peak power demand from auxiliary air-conditioning equipment (kW)	425	128	155	169	48.4
Peak space heating demand (kW)	1230	491	435	946	0
Peak water heating demand (kW)	0	404	274	339	231
Peak space cooling demand (kW)	5582	1774	2382	2041	617
Cooling-to-heating-to-power ratio	2.1/0.5/1	1.6/0.8/1	2/0.6/1	2/1.3/1	3/1.1/1

corresponding power, heating and cooling demands, as well as the cooling-to-heating-to-power ratio, for the various building types investigated. The typical daily load profiles of power, heating and cooling could differ from season to season throughout a year. It was not straightforward to show a representative daily load profile for each building type. Therefore, the summarized loadings for the different building types are provided instead.

The total capacities of the BDTS were based on the peak electrical loads of the buildings. With the utilization of the waste heat from the prime movers for cooling, the building electrical demands were smaller than those indicated in Table 2, the extent of which depended in turn on the capacities of the prime movers. Hence, repeated trials were required in order to finalize the BDTS designs. In practical considerations, several units of prime movers were normally used. The number of prime movers selected was based on the fact that any prime mover would not be operated at a part-load ratio below a presumed minimum (say 50%) throughout the year. For the reference office and retail buildings as well as the sports center, the daily peak power demands during the low-load period were mildly over half of those during the peak-load period. In this regard, two units of prime movers were used. On the other hand, the power demand profiles for the hotel and hospital buildings were substantially different since a certain amount of electricity was still required during the midnight time. In these circumstances, the adoption of three units allowed the operation of at least one set of prime movers throughout the whole year so that the part-load ratio of the BDTS was still above 50%. In order words, these two building types could operate without grid connection. To facilitate the subsequent system design, the number of absorption chillers used was the same as the number of prime movers employed. Depending on the capacity for the auxiliary cooling system (if required), multiple vapor-compression chillers might be used. Table 3 shows the final configurations of the BDTS adopted for the various building types.

The sizing of the chillers, heat exchangers and the flow rates of the pumps were based on the design temperatures as indicated previously in Figure 2. The standard component model offered by TRNSYS was employed to predict the design airflow and power demand of the cooling tower fans.

Table 3 Summarized system configurations of the BDTS for the various building types

	OF	HT	RT	HP	SC
Number of prime movers	2	3	2	3	2
Number of auxiliary vapor-compression chillers	1	2	2	2	1
Number of auxiliary water coolers	1	1	1	1	1

The fan static was taken as 200 Pa with a fan efficiency of 65%. All water pumps were assumed to have an efficiency of 60% according to EMSD (2007). Regarding the auxiliary water cooler, the sizing was based on the situation when only one set of prime movers was running. The standard component model offered by TRNSYS was used to determine the capacity of the cooling fans in the auxiliary water cooler. Again, the fan static was taken as 200 Pa with the fan efficiency being 60%. For the fan coil units used in the reference office, hotel, retail and hospital buildings, the fan static was assumed to be 250 Pa with an overall efficiency of 40% according to EMSD (2007). For the reference sports center, air handling units were employed with a fan static of 750 Pa and the fan efficiency taken as 70%. The auxiliary heaters for space heating were over-sized by 20% according to EMSD (2007) with a thermal efficiency of 90%. Tables 4 and 5 summarized the key design parameters of the CI- and SI-primed BDTS for the various building types.

4 Methodology of analysis

As previously mentioned in Section 3.2.1, an optimization study was first made to determine the load sharing strategy among the prime movers. Then, system simulations were conducted for one year using the component-based software TRNSYS. TRNSYS offers an interactive interface for building a system. Each piece of equipment is represented by a component with specified inputs and outputs which can be added and linked as desired. In this study, default parameters as adopted in the TRNSYS components were used unless otherwise specified. For the CI/SI internal combustion engines and the absorption chiller, new TRNSYS components were developed which determined the equipment performance by multi-dimensional linear interpolation through respective performance data files generated using the models mentioned in Section 2. The vapor compression chiller model from the TESS library of TRNSYS is based on a specified rated cooling capacity and rated coefficient of performance (*COP*) as key parameters. The chiller performance is calculated from respective adjustment parameters for cooling capacity and power input under different combinations of the operating conditions like cooling water entering temperature, chilled water supply temperature and part-load ratio.

To highlight the robustness of the methodology, a sensitivity analysis of the system performance to the simulation time step was performed. The total primary energy consumption (*PEC*) was adopted as the parameter for comparison. Upon completion of the sensitivity analysis, the performance of the BDTS was analyzed in details. The total *PEC* was also used to assess the energy merit of the BDTS. Here, the thermal efficiency of the grid power was taken as 40.8% with reference to the primary energy input

Table 4 Summarized key CI-primed BDTS design parameters

System design parameter	OF	HT	RT	HP	SC
Unit rated electrical output (kW)	1355	372	575	325	103
Unit rated electrical efficiency (%)	40.2	38.4	39.7	38.0	37.3
Unit rated fuel injection rate (kg/hr)	274.5	78.75	117.9	69.75	22.50
Unit rated waste heat recovered (kW)	1413	402	594	358	122
Unit rated capacity of absorption chillers (kW)	1036	279	422	248	81.3
Rated *COP* of absorption chillers	0.733	0.695	0.711	0.693	0.668
Unit rated power input of engine jacket water pump (kW)	2.243	0.728	1.010	0.656	0.216
Unit rated power input of regenerative hot water pump (kW)	11.24	3.198	4.726	2.848	0.968
Unit rated power input of cooling water pump for absorption chiller (kW)	19.48	5.421	8.085	4.822	1.615
Unit rated power input of cooling tower for absorption chiller (kW)	30.93	9.196	13.31	8.270	3.314
Unit rated power input of chilled water pump for absorption chiller (kW)	7.491	6.062	9.163	5.383	1.764
Unit rated capacity of auxiliary vapor-compression chillers (kW)	3510	468	769	648	454
Unit rated power input of cooling water pump for auxiliary chiller (kW)	33.00	4.530	7.415	6.253	4.401
Unit rated power input of cooling tower for auxiliary chiller (kW)	51.83	7.820	12.28	10.48	7.620
Unit rated power input of chilled water pump for auxiliary chiller (kW)	25.39	10.15	16.68	14.06	9.859
Unit rated power input of auxiliary water cooler (kW)	7.500	6.111	3.333	1.944	0.833
Unit rated power input of space heating water pump (kW)	14.68	5.859	5.190	11.29	NA
Total capacity of auxiliary heater for space heating (kW)	NA	491	435	1051	NA
Total capacity of auxiliary heater for water heating (kW)	NA	449	305	377	257
Total power consumption for fans (kW)	127.2	42.99	42.43	60.73	18.15

Remark: NA refers to not applicable.

Table 5 Summarized key SI-primed BDTS design parameters

System design parameter	OF	HT	RT	HP	SC
Unit rated electrical output (kW)	1400	370	574	325	102
Unit rated electrical efficiency (%)	40.0	37.5	38.3	37.5	36.2
Unit rated fuel injection rate (kg/h)	252.0	71.10	108.0	63.33	20.25
Unit rated waste heat recovered (kW)	1442	405	615	356	123
Unit rated capacity of absorption chillers (kW)	1054	282	438	247	82.1
Rated *COP* of absorption chillers	0.731	0.696	0.713	0.693	0.669
Unit rated power input of engine jacket water pump (kW)	2.307	0.744	1.062	0.648	0.228
Unit rated power input of regenerative hot water pump (kW)	11.47	3.222	4.893	2.848	0.976
Unit rated power input of cooling water pump for absorption chiller (kW)	19.86	5.464	8.381	4.822	1.629
Unit rated power input of cooling tower for absorption chiller (kW)	31.51	9.264	13.77	8.270	3.336
Unit rated power input of chilled water pump for absorption chiller (kW)	7.624	6.116	9.514	5.383	1.781
Unit rated capacity of auxiliary vapor-compression chillers (kW)	3474	464	752	648	453
Unit rated power input of cooling water pump for auxiliary chiller (kW)	32.66	4.494	7.259	6.253	4.386
Unit rated power input of cooling tower for auxiliary chiller (kW)	51.29	7.764	12.04	10.48	7.596
Unit rated power input of chilled water pump for auxiliary chiller (kW)	25.12	10.07	16.32	14.06	9.825
Unit rated power input of auxiliary water cooler (kW)	7.778	6.111	3.611	1.944	0.833
Unit rated power input of space heating water pump (kW)	14.68	5.859	5.190	11.29	NA
Total capacity of auxiliary heater for space heating (kW)	NA	491	435	1051	NA
Total capacity of auxiliary heater for water heating (kW)	NA	449	305	377	257
Total power consumption for fans (kW)	127.2	42.99	42.43	60.73	18.15

Remark: NA refers to not applicable.

according information from the major local power company (CLP 2021). Regarding the environmental issue, the parameter of total carbon dioxide emissions (*CDE*) was considered and that the carbon dioxide emissions index of the grid electricity was taken as 0.7 kg/kWh according to the information from BEAM Plus (2021). For the CCW systems with primary auxiliary heaters (except the reference office building), two cases were included, one using conventional diesel oil (DO) and the other using town gas (TG) when compared with those of the BDTS which adopted biodiesel and biogas. The carbon dioxide emissions indices of diesel oil and town gas were taken as 0.252 and 0.236 kg/kWh respectively.

The economic benefit of the BDTS was based on the simple payback (*SP*) as defined by

$$SP = \frac{\text{Additional initial cost}}{\text{Annual running cost redution}} \tag{34}$$

According to the information from the local manufacturers, the price for the biodiesel was around two times that of the normal diesel in the market. The latter was calculated based on the average import price for 2020 (CSD 2021) plus a 10% local infrastructure cost and a profit margin of 50%. Regarding the biogas, it was taken as 2/3 that of the price for town gas (HKCG 2022) from the major local gas supplier according to SCMP (2015). The electricity charge was based on the tariff scheme from the major local electricity supplier (CLP 2022).

The main advantage of using biofuels is its carbon-free nature. To assess its benefit in terms of cost saving, a carbon price should be taken into account, and the most common practice is the carbon tax. At present, there is no carbon tax in Hong Kong. Hence, the benefit of the large reduction in *CDE* for the BDTS cannot be truly reflected. According to the World Bank (2021), Sweden currently implements the carbon tax which is generally the most expensive one in the world at over USD137.0 per ton of carbon dioxide generated. For other Nordic countries, the carbon tax ranges from USD28.0 to USD73.0. Clearly, with carbon tax, the payback period can be reduced. The emission of carbon dioxide also incurs other latent impact to the society which can be expressed by a social cost (Aldy et al. 2021). Kikstra et al. (2021) computed the mean social cost of carbon dioxide ($SCCO_2$) under different modeling approaches and shared socioeconomic pathways (SSP's). According to their calculations, this cost could range from USD48.0 up to USD11787.0 per ton of carbon dioxide emitted. In this regard, consideration of the social cost can further improve the economic merit of the BDTS. Therefore, in this study, three scenarios were involved as shown below:

S1. No carbon price;
S2. Adoption of a carbon tax of USD25.0 per ton of *CDE* [an average level as exercised in United Kingdom according to the World Bank (2021)];
S3. Inclusion of a social cost of USD263.5 per ton of *CDE* which is the median value of those computed by Kikstra et al. (2021) under different combinations of the modeling approaches and SPP's.

5 Results and discussions

5.1 Optimal loading sharing strategy analysis for prime movers

With more than one prime mover in operation, it would be interesting to investigate the optimal load sharing pattern among the prime movers at different system loads. To analyze, the first step was to establish a correlation between the fuel injection ratio (*FIR*) and the part-load ratio (*PLR*) of the prime mover in which

$$FIR = \frac{FI_{\text{pm}}}{FI_{\text{pm,nom}}} \text{ and } PLR = \frac{\dot{W}_{\text{pm}}}{\dot{W}_{\text{pm,nom}}} \tag{35}$$

Here, FI_{pm} was the fuel injection rate and $\dot{W}_{\text{pm}}$ was the power output of the prime mover. The performances of the prime mover at different fuel injection ratios, ambient temperatures and engine jacket water entering temperatures were determined based on the models as mentioned in Section 3.1. Figure 8 shows the respective part-load performance curves for the BDTS for use in the reference hospital building for illustration. The corresponding part-load ratio for each fuel injection ratio was calculated by averaging over different combinations of the ambient and engine jacket water entering temperatures.

To approximate the part-load performance curves as shown in Figure 8, a cubic equation was employed which was given by

$$FIR = a_0 + a_1 PLR + a_2 PLR^2 + a_3 PLR^3 \tag{36}$$

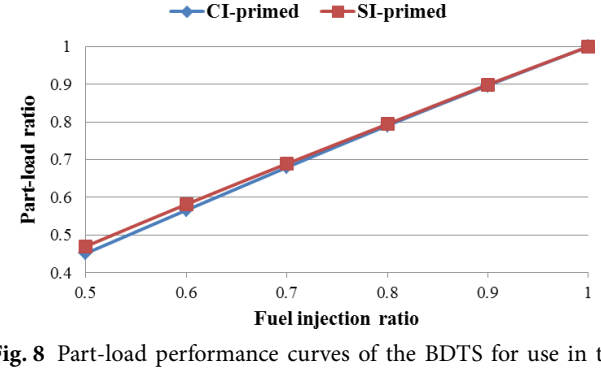

Fig. 8 Part-load performance curves of the BDTS for use in the reference hospital building

Since the part-load performance curves should pass two end points (0,0) and (1,1), Eq. (36) could be simplified to

$$FIR = (1 - a_2 - a_3)PLR + a_2 PLR^2 + a_3 PLR^3 \quad (37)$$

The two coefficients were determined by using the simplex method (Nelder and Mead 1965) as summarized in Table 6. With maximum three sets of prime movers and minimum *PLR* of 0.5, the ranges of feasible load ratio ($t\dot{W}_{demand} / \dot{W}_{pm,nom}$) corresponding to different numbers of prime movers we restricted as depicted in Figure 8.

For load ratio less than one, only one prime mover could be used. When the load ratio exceeded two, three prime movers must be used. Only when the load ratio was between 1.5 and 2 should there be two feasible numbers of prime movers. To determine the optimal load sharing, the golden search method was employed when N_{pm} = 2, while the simplex method was adopted when N_{pm} = 3. Table 7 shows the optimal total fuel injection ratios ($tFIR_{opt}$) normalized by the corresponding total fuel injection ratios based on equal load sharing ($tFIR_{els}$) at different load ratios. Clearly, the calculated $tFIR_{opt}$ was very close to the $tFIR_{els}$, which indicated that the adoption of equal load sharing among the prime movers was effective and nearly optimal. As shown in Figure 9, there are two feasible N_{pm} when the load ratio was between 1.5 and 2. By reviewing Table 7, the choice of three operating prime movers led to slightly lower values of $tFIR_{opt}/tFIR_{els}$. However, by only comparing the $tFIR_{opt}$, it was found that the selection of two operating prime movers actually offered lower fuel consumption even if the extra power consumption which resulted from the operation of more pumps was not taken into account. Consequently, the number of operating prime movers only increased when the existing ones could not meet the power demand as reflected in Eq. (29).

Table 6 Summarized coefficients for the part-load performance curves of the BDTS

System	a_2	a_3
CI-primed BDTS	−0.77256	0.40065
SI-primed BDTS	−0.50790	0.26777

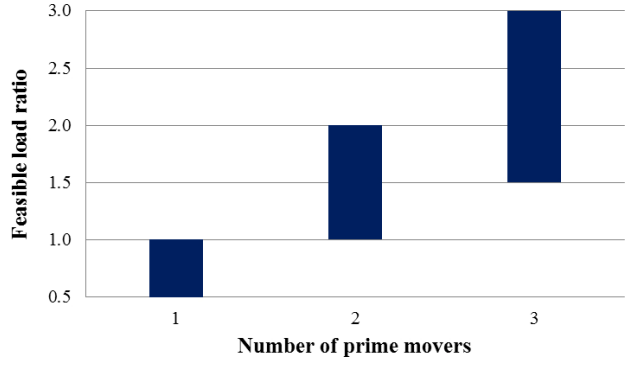

Fig. 9 Summarized feasible load ratio range at different numbers of prime movers

Table 7 Calculated normalized optimal total fuel injection ratios at different load ratios

	$tFIR_{opt}/tFIR_{els}$			
	CI-primed BDTS		SI-primed BDTS	
Load ratio	N_{pm} = 2	N_{pm} = 3	N_{pm} = 2	N_{pm} = 3
1.1	0.9995	NA	0.9997	NA
1.3	1.0000	NA	1.0000	NA
1.5	1.0000	NA	1.0000	NA
1.7	1.0000	0.9990	1.0000	0.9995
1.9	1.0000	0.9995	1.0000	0.9998
2.1	NA	1.0000	NA	1.0000
2.3	NA	1.0000	NA	1.0000
2.5	NA	1.0000	NA	1.0000
2.7	NA	1.0000	NA	1.0000

Remark: NA refers to not applicable.

5.2 Simulation time step sensitivity analysis

To demonstrate the effect of the simulation time step on the system performance, the case with the reference hospital building was selected. Figure 10 shows the variation of the simulated total *PEC* when the simulation time step was 3, 6, 10, 15, 20 and 30 minutes respectively. When the simulation time step increased from 3 to 15 minutes, the total *PEC* varied within a very narrow range. Only when the simulation time step jumped to 20 minutes should a comparatively more evident deviation of the simulated total *PEC* be found although the actual percentage difference was not high. It appeared that the use of 15 minutes should be acceptable in order to minimize the computation load.

To further differentiate the effect of the simulation time step between 3 and 15 minutes inclusive, the temperature variations at the hottest and coldest day for the bottom cubicles of the reference hospital building were tracked as shown in Figures 11 and 12. It could be found that with a

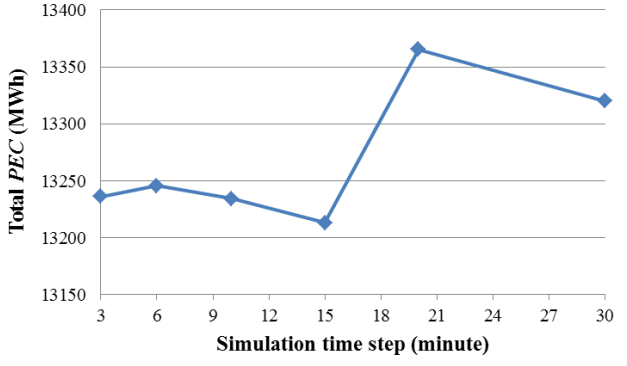

Fig. 10 Effect of the simulation time step on the year-round total *PEC* of the BDTS for use in the reference hospital building

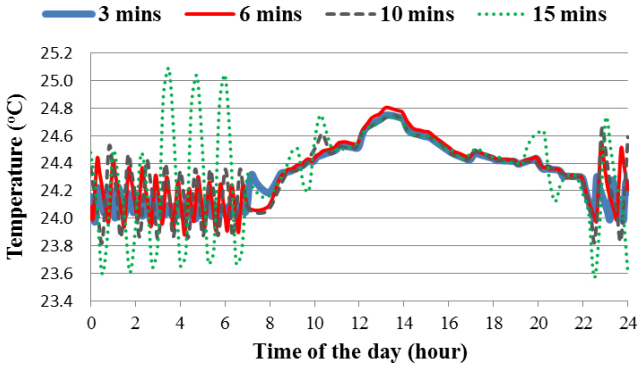

Fig. 11 Variations of the zone temperatures at the bottom cubicles during the hottest day under different simulation time steps

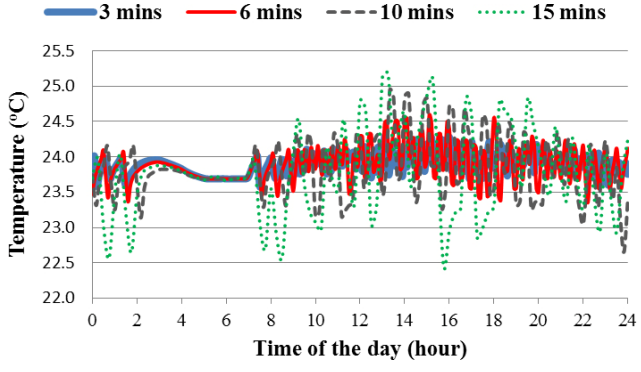

Fig. 12 Variations of the zone temperatures at the bottom cubicles during the coldest day under different simulation time steps

simulation time step of 10 minutes or higher, the oscillation of the zone temperature became more severe. This also reflected the stability and convergence of the system iteration at each simulation time step. In this regard, the selection of 6 minutes was considered the most appropriate.

5.3 Energy and environmental evaluation

Table 8 summarizes the year-round simulation results for the various BDTS cases investigated. Here, the averaged prime mover electrical efficiency (*PMEE*) was also included for comparison. Figure 13 illustrates the year-round total *PEC* for the various cases. The *PEC* saving for the CCW cases were indicated as zero for reference in Figure 13(b). In view of the *PEC* reduction percentages, the reference hotel building was the highest, followed by hospital, sports center, retails and office the lowest. The energy performance of the BDTS for use in the reference hotel building was the best because there was large heating requirement in this application with around 15% reduction in *PEC*. Although the water heating demand in the reference sports center was substantial, the lowest averaged *PMEE* in this application pushed the percentage saving in *PEC* down to the third lowest amongst the various building types investigated which measured around 10%. The application of the BDTS to the reference office building offered the lowest percentage

Table 8 Comparison of the year-round performances for various cases considered

Case	Averaged *PMEE* (%)	Total electricity consumption (MWh)	Total biofuel consumption (MWh)	Total *PEC* (MWh)	Total *CDE* (ton)
OF, CCW	NA	8410	0	20613	5887
OF, CI-primed	39.6	1087	16812	19476 (↓5.5%)	761
OF, SI-primed	39.7	1041	16947	19498 (↓5.4%)	729
HT, CCW	NA	4255	1914	12343	3461 (DO) 3430 (TG)
HT, CI-primed	37.0	0	10540	10540 (↓14.6%)	0
HT, SI-primed	36.5	0	10705	10705 (↓13.3%)	0
RT, CCW	NA	3877	1028	11367	2973 (DO) 2957 (TG)
RT, CI-primed	38.8	384	8650	9591 (↓8.9%)	269
RT, SI-primed	37.7	422	8762	9796 (↓7.0%)	295
HP, CCW	NA	4093	2213	12245	3423 (DO) 3387 (TG)
HP, CI-primed	36.6	0	11027	11027 (↓10.0%)	0
HP, SI-primed	36.6	0	11065	11065 (↓9.6%)	0
SC, CCW	NA	550	670	2018	554 (DO) 543 (TG)
SC, CI-primed	35.7	109	1544	1811 (↓10.3%)	76
SC, SI-primed	35.2	106	1571	1831 (↓9.3%)	74

Remark: NA refers to not applicable.

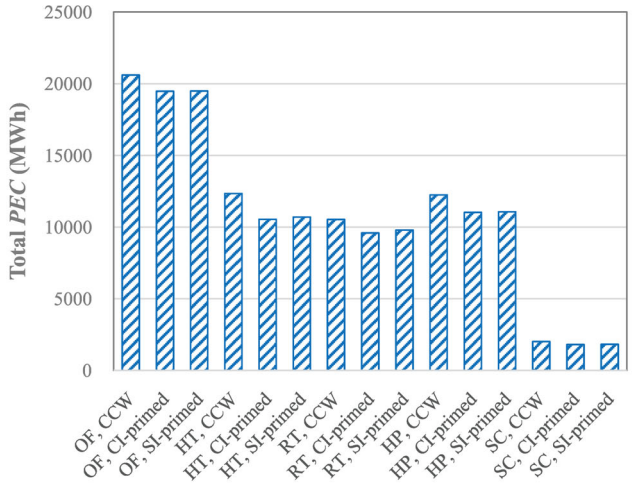

(a) Total *PEC* for the various BDTS investigated

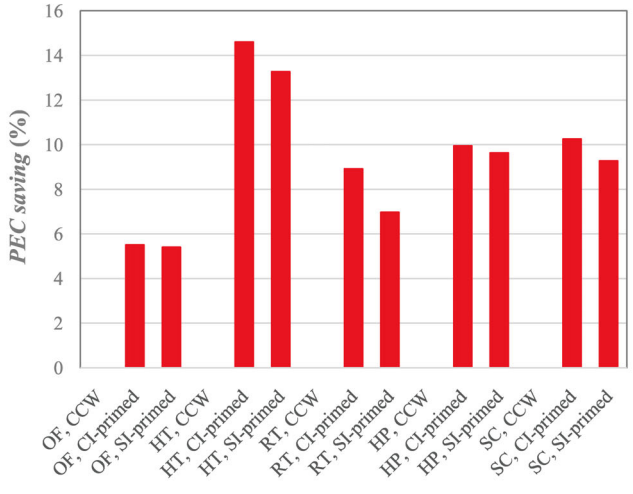

(b) *PEC* saving for the various BDTS investigated

Fig. 13 Summarized (a) total *PEC* and (b) *PEC* saving for the various BDTS investigated

reduction in *PEC*. The main reason was that in the reference office building, most of the recovered waste heat was used for space cooling as the heating demand was minimal even though the averaged *PMEE* in this application were the highest amongst the various building types considered as shown in Table 8. The large difference in the *COP's* between the absorption chiller and the conventional vapor-compression chiller substantially reduced the energy merit of utilizing the waste heat for space cooling in terms of primary energy saving. Overall speaking, the CI-primed BDTS offered higher percentage reduction in *PEC* as compared to those based on the SI-primed BDTS for all the building types analyzed.

Figure 14 indicates the respective *CDE* for the various BDTS analyzed. Again, the *CDE* reductions for the CCW cases were marked zero for reference in Figure 14(b). Clearly, the percentage reductions in *CDE* were the best for

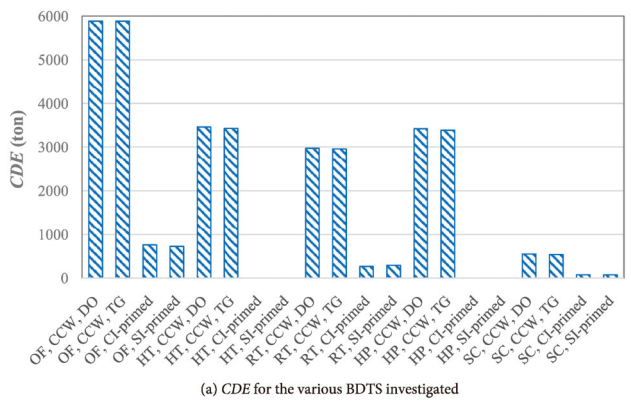

(a) *CDE* for the various BDTS investigated

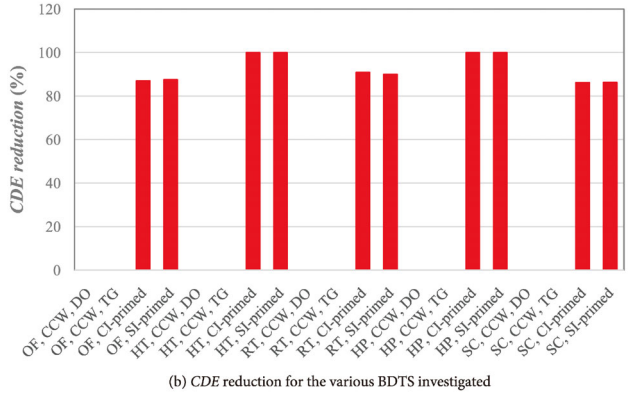

(b) *CDE* reduction for the various BDTS investigated

Fig. 14 Summarized (a) *CDE* and (b) *CDE* reduction for the various BDTS investigated

use in the reference hotel and hospital building with zero carbon emission due to their capabilities to operate without any grid connection as mentioned previously in Section 3.3. Meanwhile, the applications to the rest of building types which required auxiliary electricity from the grid managed to achieve at least 86% reduction in *CDE*. In this regard, the environmental merit of the BDTS is promising. For the reference office building and sports center, the SI-primed BDTS offered slightly higher percentage saving in *CDE*. However, the CI-primed BDTS was slightly better in the reference retail building. Meanwhile, the *CDE* of the conventional CCW systems with diesel oil or towngas for heating differed only mildly by at most 2% for the sports center.

5.4 Economical assessment

Table 9 compares the annual running cost of the BDTS with the corresponding CCW systems for the various building types analyzed under different scenarios. It was found the use of the CI-primed BDTS resulted in higher annual running cost as compared to the respective CCW systems in all the cases even with the inclusion of carbon social cost. In other word, the CI-primed BDTS were economically

infeasible. On the other hand, reductions in annual running cost were found when the SI-primed BDTS were employed without any carbon price although the saving was small for the reference office building. Nevertheless, the situation was substantially improved with the inclusion of carbon tax and carbon social cost. It highlighted that SI-primed BDTS fueled by biogas had the potential for use in a wide range of multi-storey buildings.

To further evaluate the economic merit of the SI-primed BDTS, the respective payback periods were determined. Table 10 summarizes the corresponding initial cost of the SI-primed BDTS and CCW systems for the various building types analyzed and the respective *SP's* under different situations. The values were based on the local market prices in 2021. From Table 10, the *SP's* were the lowest for use in the reference hotel building under all the scenarios considered, which measured 5.9 years even in the absence of any carbon price, and fell to less than 1 year with the carbon social cost taken into account. This was followed by the application in the reference hospital building. In both types of buildings, the water heating demand was high and that zero-carbon operation could be achieved. On the other hand, the situation was the worst for use in the reference office building with no water heating requirement. With carbon tax, *SP* was 15.1 years but dropped drastically to less than 2 years by taking the carbon social cost into account.

Table 9 Comparison of annual running cost between BDTS and CCW systems for the various building types investigated

Case	Annual running cost (million USD)		
	S1	S2	S3
OF, CCW	1.528	1.675	1.727
OF, CI-primed	2.822	2.841	2.847
OF, SI-primed	1.525	1.543	1.549
HT, CCW	0.922 (DO) 0.922 (TG)	1.009 (DO) 1.085 (TG)	1.039 (DO) 1.115 (TG)
HT, CI-primed	1.645	1.645	1.645
HT, SI-primed	0.844	0.844	0.844
RT, CCW	0.784 (DO) 0.826 (TG)	0.859 (DO) 0.900 (TG)	0.885 (DO) 0.926 (TG)
RT, CI-primed	1.420	1.427	1.429
RT, SI-primed	0.767	0.774	0.777
HP, CCW	0.916 (DO) 1.005 (TG)	1.002 (DO) 1.090 (TG)	1.032 (DO) 1.120 (TG)
HP, CI-primed	1.721	1.721	1.721
HP, SI-primed	0.872	0.872	0.872
SC, CCW	0.152 (DO) 0.179 (TG)	0.166 (DO) 0.193 (TG)	0.171 (DO) 0.197 (TG)
SC, CI-primed	0.261	0.263	0.263
SC, SI-primed	0.143	0.145	0.146

Table 10 Summarized initial cost and simple paybacks of the SI-primed BDTS and CCW systems for the various building types investigated

Building type	Initial cost (million USD)		Simple payback (Year)		
	CCW	BDTS	S1	S2	S3
OF	1.564	3.564	621	15.1	1.3
HT	0.545	1.462	5.9	3.8	0.8
RT	0.718	1.705	16.8	7.9	1.2
HP	0.545	1.462	6.9	4.2	0.8
SC	0.192	0.462	7.5	5.6	1.6

As mentioned in Section 4, the carbon tax and carbon cost varied from place to place. Meanwhile, the price for biofuels were generally more stable than the fossil fuels which fluctuated vigorously in recent years under the threat of COVID 19. Hence, it would be useful to investigate how the carbon prices affected the paybacks only. Figures 15–16 depict the impact of carbon tax and carbon cost variation on the corresponding paybacks. A fluctuation of ±50% was considered with reference to those wide ranges previously stated in Section 4. It could be found that the impact of the carbon tax under S3 was very limited. This was due to the fact that the carbon cost stated in Section 4 was much higher than the carbon tax. Under S2, the impact of carbon tax differed substantially among the various building type considered. The *SP* in the office building was more sensitive to the carbon tax which nearly doubled with a 50% decrease in the carbon tax. Meanwhile, the impact was the least for the sports center which only increased by 14% when the carbon tax decreased by 50%. Regarding the carbon

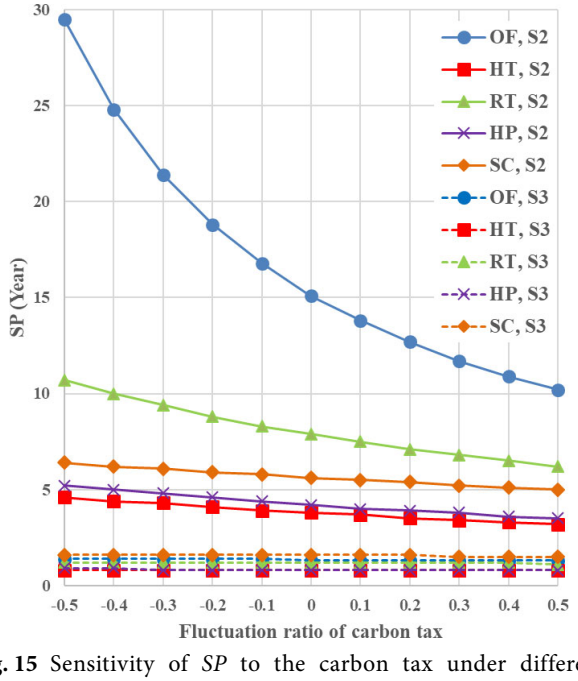

Fig. 15 Sensitivity of *SP* to the carbon tax under different scenarios

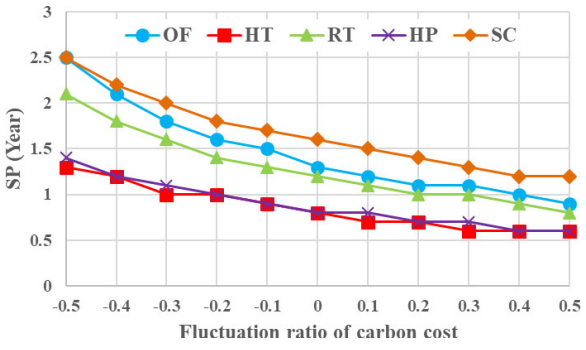

Fig. 16 Sensitivity of *SP* to the carbon cost under S3

cost under S3, the sensitivity of *SP* varied to a lesser extent as compared to the carbon price under S2. Although the impact of carbon price to the *SP* of office building was similar to that of the carbon tax under S2, the corresponding sensitivity of carbon price to the *SP* of sports center was much higher than that of the carbon tax in S2. With the carbon price ranged from −50% to +50% of the value stated in Section 4, the *SP* of sports center decreased from 2.5 to 1.2 years as compared to the variation of *SP* from 6.4 to 5 years based on the same fluctuation range for the carbon tax. Except for the office building, the *SP* under S2 almost fell below 10 years and that the *SP* under S3 was at most 2.5 for all the building types and carbon tax considered. It can thus be concluded that SI-primed BDTS are feasible low-carbon alternatives for sustainable use in multi-storey buildings in Hong Kong.

6 Conclusion

A comprehensive study has been conducted to evaluate the application potential of BDTS for the various non-residential building types, including office, hotel, retail, hospital and sports center in the subtropical Hong Kong using TRNSYS. Biodiesel and biogas were provided to the CI- and SI-primed BDTS respectively. Beforehand, a sensitivity analysis of the simulation time step was conducted for the reference hospital building to determine the optimal simulation time step based on the total *PEC*. It was found that BDTS had definite energy and environmental merits compared to the corresponding conventional systems in all types of buildings investigated, with the reference hotel building the highest while the reference office building the lowest. The CI- and SI-primed BDTS for the reference hotel building could have *PEC* saving of 14.6% and 13.3% respectively. Due to the nature of 24/7 operation of the reference hotel and hospital buildings, these two types of BDTS could achieve full 100% *CDE* reduction without the need for grid connection. In case economic assessment was conducted against the respective conventional systems, the CI-primed BDTS were not viable even in running cost according to the biodiesel price in Hong Kong. Nevertheless, the SI-primed BDTS, which used the biogas, were able to have saving in the annual running cost, hence payback periods could be worked out. Again, it was found that the reference hotel building with SI-primed BDTS had the shortest payback periods in different scenarios: 5.9 years in the absence of carbon price, 3.8 years when adopting carbon tax, and less than 1 year if social cost involved. However, in the scenario of no carbon price, the SI-primed BDTS for the reference office and retail buildings would be unfavorable. If the social cost was included, the payback could be reduced to 2 years or less for all types of non-residential buildings. Consequently, the SI-primed BDTS could have energy, environmental and economic advantages in the non-residential building types when carbon price was considered. Apparently, this has provided a tangible support of low carbon or even zero carbon building design in the subtropical climate.

Acknowledgements

The work described in this paper was fully supported by a grant from City University of Hong Kong (Strategic Research Grant, Project No. 7005033).

References

Aldy JE, Kotchen MJ, Stavins RN, et al. (2021). Keep climate policy focused on the social cost of carbon: A proposed shift away from the SCC is ill advised. *Science*, 353(6557): 850–852.

Al-Sulaiman FA, Dincer I, Hamdullahpur F (2010). Energy analysis of a trigeneration plant based on solid oxide fuel cell and organic Rankine cycle. *International Journal of Hydrogen Energy*, 35: 5104–5113.

BEAM Plus (2021). BEAM Plus for New Buildings Version 2.0. BEAM Society Limited.

Chan ALS, Chow TT, Fong SKF, Lin JZ (2006). Generation of a typical meteorological year for Hong Kong. *Energy Conversion and Management*, 47: 87–96.

Chen Y, Zhang T, Yang H, et al. (2016a). Study on energy and economic benefits of converting a combined heating and power system to a tri-generation system for sewage treatment plants in subtropical area. *Applied Thermal Engineering*, 94: 24–39.

Chen Y, Luo Y, Yang H (2016b). An optimization method for design and operation of combined cooling, heating, and power systems toward a smart grid. *Science and Technology for the Built Environment*, 22: 766–782.

CLP (2021). CLP Holdings 2020 Annual Report. CLP Holdings Limited.

CLP (2022). Electricity Tariff. Available at https://www.clp.com.hk/content/dam/clphk/documents/tariff-adjustment-2022/Tariff%20Table%20-%20English%20(2022-01-01).pdf. Assessed on 18 Oct 2022.

CSD (2021). Hong Kong Energy Statistics 2020 Annual Report. Census and Statistics Department, the Hong Kong Special Administrative Region.

Dehghani MJ, Yoo CK (2020). Modeling and extensive analysis of the energy and economics of cooling, heat, and power trigeneration (CCHP) from textile wastewater for industrial low-grade heat recovery. *Energy Conversion and Management*, 205: 112451.

EB (2015). Energy Saving Plan for Hong Kong's Built Environment 2015–2025+. Environmental Bureau, the Hong Kong Special Administrative Region.

EB (2021). Hong Kong's Climate Action Plan 2050. Environmental Bureau, the Hong Kong Special Administrative Region.

EMSD (2007). Guidelines on Performance-based Building Energy Code. Electrical and Mechanical Services Department, the Hong Kong Special Administrative Region.

EMSD (2012). Code of Practice for Energy Efficiency of Building Services Installation. Electrical and Mechanical Services Department, the Hong Kong Special Administrative Region.

Florides GA, Kalogirou SA, Tassou SA, et al. (2003). Design and construction of a LiBr-water absorption machine. *Energy Conversion and Management*, 44: 2483–2508.

Fong KF, Chow TT, Lee CK, et al. (2010). Comparative study of different solar cooling systems for buildings in subtropical city. *Solar Energy*, 84: 227–244.

Fong KF, Lee CK, Chow TT (2012). Comparative study of solar cooling systems with building-integrated solar collectors for use in sub-tropical regions like Hong Kong. *Applied Energy*, 90: 189–195.

Fong KF, Lee CK (2015). Performance analysis of internal-combustion-engine primed trigeneration systems for use in high-rise office buildings in Hong Kong. *Applied Energy*, 160: 793–801.

Fong KF, Lee CK (2017). Dynamic performances of trigeneration systems using different prime movers for high-rise building application: A comparative study. *Building Simulation*, 10: 509–523.

Gazda W, Stanek W (2016). Energy and environmental assessment of integrated biogas trigeneration and photovoltaic plant as more sustainable industrial system. *Applied Energy*, 169: 138–149.

Herold KE, Radermacher R, Klein SA (2016). Absorption chillers and heat pumps. Boca Raton, FL, USA: CRC Press.

HKCG (2022). Tariff. The Hong Kong and China Gas Company Limited. Available at https://www.towngas.com/Eng/Cust/Household/CustService/Tariff.aspx. Last accessed on 18 October 2022.

Hossain AK, Thorpe R, Critoph RE, et al. (2011). Development of a small-scale trigeneration plant based on a CI engine fuelled by neat non-edible plant oil. *Journal of Scientific & Industrial Research*, 70: 688–693.

Kikstra JS, Waidelich P, Rising J, et al. (2021). The social cost of carbon dioxide under climate-economy feedbacks and temperature variability. *Environmental Research Letters*, 16: 094037.

Lee CK, Lam HN (2014). Simplified explicit calculation algorithms for determining the performance of refrigerant coils in vapour-compression systems. *International Journal of Refrigeration*, 38: 178–188.

Li G (2012). Hong Kong's first zero carbon building and its key engineering considerations. In: Proceedings of the 11th Annual Power Symposium 2012, Hong Kong, China.

Meyers S, Schmitt B, Chester-Jones M, et al. (2016). Energy efficiency, carbon emissions, and measures towards their improvement in the food and beverage sector for six European countries. *Energy*, 104: 266–283.

Nelder JA, Mead R (1965). A simplex method for function minimization. *The Computer Journal*, 7: 308–313.

Nourin FN, Abbas AI, Qandil MD, et al. (2021). Analytical study to use the excess digester gas of wastewater treatment plants. *Journal of Energy Resources Technology*, 143: 012104.

Nowak O, Enderle P, Varbanov P (2015). Ways to optimize the energy balance of municipal wastewater systems: lessons learned from Austrian applications. *Journal of Cleaner Production*, 88: 125–131.

OPARK1 (2020). Available at https://www.opark.gov.hk/en/index.php. Accessed 18 October 2022.

Parise JAR, Castillo Martínez LC, Marques RP, et al. (2011). A study of the thermodynamic performance and CO_2 emissions of a vapour compression bio-trigeneration system. *Applied Thermal Engineering*, 31: 1411–1420.

Ren H, Zhou W, Nakagami K, et al. (2010). Integrated design and evaluation of biomass energy system taking into consideration demand side characteristics. *Energy*, 35: 2210–2222.

SCMP (2015). South China Morning Post. Available at http://www.scmp.com/news/hong-kong/article/1681671/nethersole-hospital-use-methane-gas-landfill-green-power-plan. Accessed on 18 October 2022.

Taseli BK, Kilkis B (2016). Ecological sanitation, organic animal farm, and cogeneration: closing the loop in achieving sustainable development—A concept study with on-site biogas fueled trigeneration retrofit in a 900-bed university hospital. *Energy and Buildings*, 129: 102–119.

the World Bank (2021). Carbon Pricing Dashboard. Available at https://carbonpricingdashboard.worldbank.org/map_data. Accessed on 18 October 2022.

TRNSYS (2011). TRNSYS 17, a TRaNsient SYstem Simulation program. The Solar Energy Laboratory, University of Wisconsin-Madison, USA.

Wang Y, Huang Y, Roskilly AP, et al. (2010). Trigeneration running with raw jatropha oil. *Fuel Processing Technology*, 91: 348–353.

Wang RZ, Yu X, Ge TS, et al. (2013a). The present and future of residential refrigeration, power generation and energy storage. *Applied Thermal Engineering*, 53: 256–270.

Wang Y, Ronilaya F, Chen X, et al. (2013b). Modelling and simulation of a distributed power generation system with energy storage to meet dynamic household electricity demand. *Applied Thermal Engineering*, 50: 523–535.

Wu D, Roskilly AP, Yu H (2013). Croton megalocarpus oil-fired micro-trigeneration prototype for remote and self-contained applications: experimental assessment of its performance and gaseous and particulate emissions. *Interface Focus*, 3: 20120041.

Wu D, Chen J, Roskilly AP (2015). Phase change material thermal storage for biofuel preheating in micro trigeneration application: A numerical study. *Applied Energy*, 137: 832–844.

ZCB (2022). Zero Carbon Building. Available at https://zcp.cic.hk/eng/home. Accessed 18 October 2022.